Physical roles of Interstellar-origin Pickup Ions at the Heliospheric Termination Shock: Impact on the Shock Front Microstructures and Nonstationarity

Bertrand Lembège, Zhongwei Yang

The Astrophysical Journal, 827:73 (16pp), 2016 August 10 doi:10.3847/0004-637X/827/1/73

PHYSICAL ROLES OF INTERSTELLAR-ORIGIN PICKUP IONS AT THE HELIOSPHERIC TERMINATION SHOCK: IMPACT ON THE SHOCK FRONT MICROSTRUCTURES AND NONSTATIONARITY

Bertrand Lembège[1] and Zhongwei Yang[2]
[1] LATMOS/IPSL/UVSQ/CNRS, F-78280 Guyancourt, France; bertrand.lembege@latmos.ipsl.fr
[2] State Key Laboratory of Space Weather, National Space Science Center, Chinese Academy of Sciences, Beijing 100190, China; zwyang@spaceweather.ac.cn
Received 2016 March 7; revised 2016 June 1; accepted 2016 June 5; published 2016 August 9

ABSTRACT

The nonstationary dynamics of the heliospheric termination shock in the presence of pickup ions (PUI) is analyzed by using a one-dimensional particle-in-cell simulation code. This work initially stimulated by *Voyager 2* data focusses on this nonstationarity for different percentages of PUIs and for different Alfvén Mach numbers M_A. Solar wind ions (SWIs) and PUIs are described, respectively, as Maxwellian and shell distributions (with a zero/finite thickness). For a moderate M_A, present results show that (1) the shock front is still nonstationary even in the presence of 25% of PUIs; its instantaneous velocity varies, which is in favor for shock multicrossing; (2) the presence of PUIs tends to smooth out the time fluctuations of field amplitude and of microstructure widths at the front and overshoot; (3) the shock has a multiple overshoot, which is analyzed by identifying the contributions of SWIs and the PUIs; (4) as the PUI percentage increases, the shock moves faster and the downstream compression becomes weaker, which is explained by a Rankine–Hugoniot model; (5) the reflection rate of SWIs and PUIs decreases as the PUI percentage increases; (6) the shock structure is almost insensitive to the shell thickness; and (7) for the PUIs dominated shock case (PUI = 55%), the shock becomes stationary. However, for higher M_A regime, the front nonstationarity persists even in the PUI = 55% case. In summary, high M_A regime allows to compensate the smoothing of the microstructures and the time fluctuations of the shock front brought by the presence of PUIs.

Key words: acceleration of particles – plasmas – shock waves – Sun: heliosphere

1. INTRODUCTION

Collisionless shocks are of great interest since, within the shock transition, the bulk energy of the plasma is converted into thermal energy in absence of particle binary collisions (Tidman & Krall 1971; Lembège et al. 2004; Burgess et al. 2005). The terrestrial bow shock has received a lot of attention since the early works of Axford (1962 and references therein, for theoretical predictions) and of Ness et al. (1964, for the first in situ detection in space). As the first frontier of our heliospheric system, the collisionless heliospheric termination shock (TS) representing the transition between the supersonic solar wind and the subsonic heliosheath has been crossed by *Voyager 1* (*V1*) and *Voyager 2* (V2) spacecraft. So far, fortunately, both the magnetometer (Burlaga et al. 2008) and plasma instruments (Richardson et al. 2008) on *V2* work well (the Plasma Science instrument on *V1* failed in 1980 before the TS crossing; Stone et al. 2005). A single crossing of the shock front was expected, but *V2* data reveals multi-crossings. Burlaga et al. (2008) have suggested that it could possibly be due to the self-reformation of the TS (Lembège & Dawson 1987; Lembège & Savoini 1992). However, many questions on the TS nonstationarity still persist, and its impact on the energy partition between the different particle species needs to be clarified.

The TS is generally believed to be quasi-perpendicular at most heliospheric latitudes because of the shock's large heliocentric distance and the Parker spiral structure of the heliospheric magnetic field. Burlaga et al. (2008) reported microstructures in the magnetic field of the TS during its multi-crossings (on 2007 August 31–September 1 at a distance of 83.7 au from the Sun, where 1 au = 146×10^6 Km is the Earth–Sun distance). *V2* data present clear-cut foot, ramp, overshoot–undershoot structures, which are typical features of a supercritical quasi-perpendicular shock. It has been suggested that this shock may differ from other shocks because of the relatively large fraction of pickup ions (PUIs). PUIs are neutral atoms of interstellar-origin that are ionized in the heliosphere, picked up and convected back by the expanding solar wind. The pickup hydrogen population is expected to be the dominant pickup species at the TS because the percentage of pickup H^+ to solar wind ions (SWIs) at 50 au is estimated to be 10% and increases linearly with distance from the Sun (Vasyliunas & Siscoe 1976). The estimated percentage of pickup H^+ at the TS is of the order of 25% of the SWI density. The compression ratio and temperature of the SWIs in the heliosheath are very low. Richardson et al. (2008) have suggested that most of the upstream plasma bulk energy is transferred to the PUIs (throughout the text, we will use SWIs and PUIs to refer the H+ SWIs and the H+ PUIs respectively). Zank et al. (2010) have suggested that the microphysics of the TS may play a key role in determining the shape of the total downstream (or heliosheath) proton distribution. These works gave us the motivation to study the impact of the turbulence created by the self-reformation on the local ion velocity distribution measured in the downstream region. However, as a first step, the present work is focused on a detailed analysis of the combined impact of the PUIs (in terms of percentage and of the PUIs shell distribution thickness) and of the shock front nonstationarity on the microstructures of a supercritical shock approaching the TS conditions.

The microstructures of the TS have been studied by hybrid and/or full particle-in-cell (PIC) simulations self-consistently including PUIs. By using a hybrid code, Liewer et al. (1993) investigated the impact of PUIs on the TS for the first time. They found that the PUIs can lead to the formation of an extended foot of length, approximately equal to the gyroradius

of the PUIs. More recently, the dependency of energy partition in the presence of PUIs (where the percentage of PUIs ranges from 0 to 40) was further considered using one-dimensional (1D) hybrid simulations by Wu et al. (2009) and it was pointed out that the downstream thermal energy ratio of PUIs $\eta_{\rm PUI} = {\rm PUI\%}(T_{\rm d}^{\rm PUI} - T_{\rm u}^{\rm PUI})/[{\rm PUI\%}(T_{\rm d}^{\rm PUI} - T_{\rm u}^{\rm PUI}) + (100–{\rm PUI\%})(T_{\rm d}^{\rm SWI} - T_{\rm u}^{\rm SWI})]$ is about 87% (for the case where the percentage of PUI, "PUI%" throughout the text, equals 25), which is close to the energy fraction gain (>84%) for PUIs inferred from the *V2* observations by Richardson et al. (2008). However, electron dynamics and its coupling with ion dynamics should also be taken into account in order to fully understand energy dissipation across a shock front.

PIC simulations of the TS started about 10 years ago (Chapman et al. 2005; Lee et al. 2005). In contrast to hybrid simulations, both electron and ion populations are taken into account as individual particles in PIC simulations, and the electrostatic potential jump at the ramp with a width of a few electron inertial lengths has been self-consistently reproduced (Matsukiyo et al. 2007). Matsukiyo & Scholer (2011) have investigated the impact of PUIs on the TS by using a 1D PIC code. An extended foot due to reflected PUIs is clearly evidenced similar to that mentioned in early hybrid simulations (Liewer et al. 1993). They have found that in the 30% PUIs case, about 90% of the total thermal energy gain in the downstream shocked region is attributed to the PUIs, while only a little under 10% to the SWIs. The energy gain of PUIs is a little higher than that calculated in previous hybrid simulations (Wu et al. 2009, 2010) due to the ramp width obtained in the 1D PIC simulation, which scales over a few electron inertial lengths. Furthermore, they mentioned that the PUIs can be reflected not only at the ramp but also at the extended foot. Recently, Matsukiyo & Scholer (2014) have extended their work, and have discussed the particle acceleration mechanisms at the front of the TS. Electron and PUI shock drift acceleration is evidenced and no evidence for the shock surfing acceleration of PUIs could be found. However, the PUIs used in previous PIC simulations are described by a thin-shell distribution (zero thickness of the shell), which may be a good approximation immediately after pickup of the ionized interstellar neutrals in the solar wind. The observed partial filling of the spherical shell distribution results from adiabatic cooling of the pickup ions as the solar wind expands (Mobius et al. 1988; Burrows et al. 2010). The underlying mechanisms of how PUIs with a filled-in shell distribution (finite—instead of zero—thickness of the shell) affect the microstructures and the nonstationarity of the TS still remain unclear.

In this paper, by separating incident ions into reflected (R) and directly transmitted (DT) parts with the help of the automatic separation method (ASM; Yang et al. 2009) inspired by an early work of Burgess et al. (1989), we investigate the impact of PUIs on the shock front self-reformation, on the microstructures and the density profiles of the SWI/PUI population of the TS. Let us briefly review the ASM procedure used to identify the reflected (R). Two conditions must be satisfied: after being reflected (1) their velocity component $v_{\rm x}$ is larger than the shock front velocity $v_{\rm shock}$ (along the x axis) and (2) they are located upstream from the ramp ($x_{\rm i} > x_{\rm ramp}$). It is important to note that, when applying the criteria mentioned above ($x_{\rm i} > x_{\rm ramp}$), the turning point of reflected ions can take place anywhere within the front without any a priori indication. Even an ion that has its turning point behind the ramp and reaches the ramp after turning toward upstream, will be selected as a reflected ion. Main questions addressed herein are: (1) Does the self-reformation persist in the presence of a noticeable percentage of PUIs? If yes, how are the microstructures of the shock front distorted in time? (2) What is the impact of different Mach number regimes versus different PUI percentages on these microstructures? And (3) what is the impact of the PUI shell thickness on the results? The paper is organized as follows. In Section 2, we briefly describe the numerical simulation conditions. The impact of the different percentages of PUIs and the nonstationarity of the TS on the scales and the local amplitude of the shock microstructures is detailed in Section 3 for a moderate Mach number regime. Section 4 presents a comparative analysis between moderate/high Mach number cases. The main features of the SWI-dominated and PUI-dominated shocks are presented in Section 5. The impact of the thickness of the PUI velocity shell distribution on the microstructures of TS, on its self-reformation and for different PUI% is studied is Section 6. The discussion of the "supersonic" plasma flow observed by *V2* (Richardson et al. 2008) in the downstream region of the TS, the interpretation of shock front multicrossing, and a comparison with previous works are presented in Section 7. Conclusions are summarized in Section 8.

2. SIMULATION MODEL

We use a 1D electromagnetic PIC code to simulate the evolving structure of a supercritical, collisionless, perpendicular shock. Herein, the shock is produced by the injection method as in previous PIC simulations (Lee et al. 2005; Matsukiyo et al. 2007; Yang et al. 2012a). In order to reproduce self-consistently the impacts of PUIs, three particle species are introduced within our PIC code: electrons, SWIs, and PUIs. All particles are injected on the left-hand side of the simulation box with a inflow/upstream drift speed $V_{\rm inj}$, and are reflected at the other end. The distribution functions for the SWIs and electrons are Maxwellian. PUIs are distributed on a sphere in velocity space centered at $V_{\rm inj}$ with radius $V_{\rm shell}$ as in earlier works (Lee et al. 2005; Matsukiyo & Scholer 2011). The shock front builds up and moves with a speed $V_{\rm ref}$ from the right-hand to the left-hand side along the x axis. The upstream Alfvénic Mach number of the shock is $M_{\rm A} = (V_{\rm inj} + V_{\rm ref})/V_{\rm A}$, where the Alfvén speed $V_{\rm A}$ is equal to one. The ambiant magnetic field directed along the y direction is $|B_0| = 1$. All basic parameters are as follows. Plasma box size length $L_{\rm x} = 80c/\omega_{\rm pi}$ for all different Mach number cases of concern herein; light velocity $c = 20$, mass ratio $m_{\rm i}/m_{\rm e} = 100$, and the electron plasma to cyclotron frequency ratio $\omega_{\rm pe}/\Omega_{\rm ce} = 2$ (from Table 2). The SWI beta $\beta_{\rm i} = 0.04$ (ratio of the ion kinetic pressure over the magnetic pressure), which is inferred from *Voyager* data for TS-3 (Burlaga et al. 2008). Electron beta $\beta_{\rm e} = 0.5$ is chosen as in previous PIC simulations (Lee et al. 2005). Initially, 200 particles (for each specie) are used in a cell. The upstream plasma is quasi-neutral, i.e., $n_{\rm e} = n_{\rm i}$, where $n_{\rm i} = n_{\rm SWI} + n_{\rm PUI} = N_{\rm SWI} \times {\rm SWI\%} + N_{\rm PUI} \times {\rm PUI\%}$, where $n_{\rm e}$, $n_{\rm i}$, $n_{\rm SWI}$, and $n_{\rm PUI}$ are the densities of the electrons (subscript "e"), of the total ions (subscript "i"), of the SWIs (subscript "SWI"), and of the PUIs (subscript "PUI"), respectively. $N_{\rm SWI}$, $N_{\rm PUI}$, SWI%, and PUI% are the counts of each species of ions and their relatively weighted percentage in the PIC simulation respectively. The simulation code includes an equal number of particles (hence $N_{\rm SWI} = N_{\rm PUI}$), but the

Table 1
List of the Different Runs of Concern in the Study with the Main Parameters Differentiating Each Run

	PUI				
	PUI%	d/V_{shell}	V_{inj}	M_A	T_{ref}/Ω_{ci}
Run 1	0	0	3	4.78	1.73
Run 2	10	0	3	4.99	1.54
Run 3	25	0	3	5.26	1.40
Run 4	55	0	3	6.01	No
Run 5	0	0	6	9.06	1.63
Run 6	10	0	6	9.08	1.50
Run 7	25	0	6	9.11	1.36
Run 8	55	0	6	9.52	1.19
Run 9	25	0.2	3	5.20	1.41
Run 10	25	0.5	3	5.15	1.43
Run 11	25	1	3	5.09	1.47
Run 12	25	0.2	6	9.07	1.44
Run 13	25	0.5	6	9.02	1.46
Run 14	25	1	6	8.97	1.50

particle weight is changed in order to achieve different densities. In this paper, we perform four groups of runs (labeled 1–4, 5–8, 9–11, and 12–14 respectively). The main plasma parameters differentiating each group are summarized in Table 1. All upstream plasma parameters common to the different runs are detailed in Table 2.

3. SIMULATION RESULTS: NONSTATIONARITY OF THE SHOCK FRONT FOR A MODERATE MACH REGIME ($M_A \sim 5$)

First, we study in detail the microstructures of the shock front in the presence of PUIs by analyzing the self-consistent density profiles of the SWI and PUI populations. Figure 1(c) shows the phase space plots of SWIs at one particular time ($t = 7.8\ \Omega_{ci}^{-1}$) for the shock in the presence of 10% PUIs (run 2). Components of the main magnetic field B_y (blue curve) and of the cross-shock field E_x (red curve) are shown for reference and shifted to the bottom of each plot. The magnetic field B_y profile exhibits a well defined PUI extended foot, an SWI foot, a ramp, and overshoot structures. The cross-shock electric field strength $|E_x|$ reaches its maximum at the ramp (vertical dashed) where the magnetic field ramp presents an inflexion point. In Figure 1(c), the incident SWIs are separated into two parts: reflected R-SWIs (red dots) and directly transmitted DT-SWIs (black dots) as in Yang et al. (2009). It is clearly evidenced that the reflected SWIs form the narrow SWI foot (blue area). Similar plots for PUIs are shown in Figure 1(d). In the same way, the incident PUIs can also be separated into two parts: reflected R-PUI (red dots) and directly transmitted DT-PUI (black dots). The reflected PUIs suffer a large gyromotion ahead of the ramp and form the extended PUI foot (green area). For both SWIs and PUIs in the downstream region, the reflected population is more energetic than the directly transmitted one. For comparison, Figures 1(a) and (b) show similar plots for the case without PUIs (0%) and are used as reference; PUIs in Figure 1(b) are test particles (with the same injection conditions as for Figures 1(c) and (d)) used for comparing their dynamics when interacting with the self-consistent shock profiles obtained when excluding or including the presence of PUIs.

Table 2
Upstream Plasma Parameters Defined for the 1D- PIC Simulation and Common to All Runs

Parameter	Description	Electrons	SWIs	PUIs
v_{th}	Thermal velocity	7.07	0.2	Shell distribution
λ_D	Debye length	0.035	0.0071	
ρ_c	Gyroradius	0.0707	0.2	
c/ω_p	Inertial length	0.1	1	
ω_c	Gyro-frequency	100	1	
ω_p	Plasma frequency	200	20	
τ_c	Gyro-period	0.01	1	
β	Plasma beta	0.5	0.04	

We further quantitatively analyze the contributions of each population to the downstream structure of the TS front (run 3, PUI% = 25) as shown in Figure 2 (left column). We again divide each SWI and PUI population into two parts (R and DT parts) and calculate their density profiles shown, respectively, in Figures 2(b) and (c) for SWIs and PUIs; these profiles are reported in Figure 2(a) and are compared with the total ion density (green curve) and the magnetic field (dark curve), which are quite similar; the multiple overshoot structure is identified by arrows "O1," "O2," and "O3." This comparison allows us to stress out the following features. (1) Overshoots persist even in the presence of a noticeable percentage of PUIs and are mainly supported by the gyrating DT-SWIs. (2) At some time, the R-SWIs (red curve in panel (b)) slightly contribute during their gyromotion downstream to a sublet of peaks "O2" and "O3," which merge into each other at later times as the SWIs propagate further downstream. (3) PUIs have downstream gyromotion (immediately behind the front) similar to that of SWIs, but no PUIs contribute to the different overshoots at any time of the run because of their relatively low downstream density (cyan curve in plot (a)). (4) The downstream density profiles of R-PUIs and DT-PUIs (plot (c)) are anticorrelated with each other, which is not the case between the profiles of R-SWIs and DT-SWIs (plot (b)). (5) The total density profile of PUIs increases with the PUI% in the extended foot but do not present any jump when crossing the shock front and stays approximately around the same value when penetrating downstream (plot (c)). An animation of Figure 2 (not shown here) confirms that the overall microstructure of the shock front stays mainly controlled at any time by the DT-SWIs not only at the front ("O1") but also further downstream (overshoots "O2" and "O3"). Note that overshoots O1, O2, and O3 can also be identified in Figures 1(a)–(b), but these are exclusively due to SWIs since PUI% = 0. By dividing again the SWI population into R and DT parts, a complementary analysis of the corresponding density profiles (for each population) and magnetic field profile (results not shown herein) clearly shows that O1, O2, and O3 are mainly supported by the DT-SWIs.

Second, we examine the impact of the relative percentage of PUIs on the shock front self-reformation. An overview of runs 1 (0% PUIs), 2 (10% PUIs), and 3 (25% PUIs) shows the time stackplots of the main magnetic field B_y (Figure 3). In the absence of PUIs (Figure 3(a)), the shock front is characterized by a self-reformation process (time modulation of "O1") with a cyclic period of about 1.73 Ω_{ci}^{-1} (measured between two successive vertical black arrows) where Ω_{ci} is the upstream ion gyro-frequency. The bulk velocity of the ions injected from the

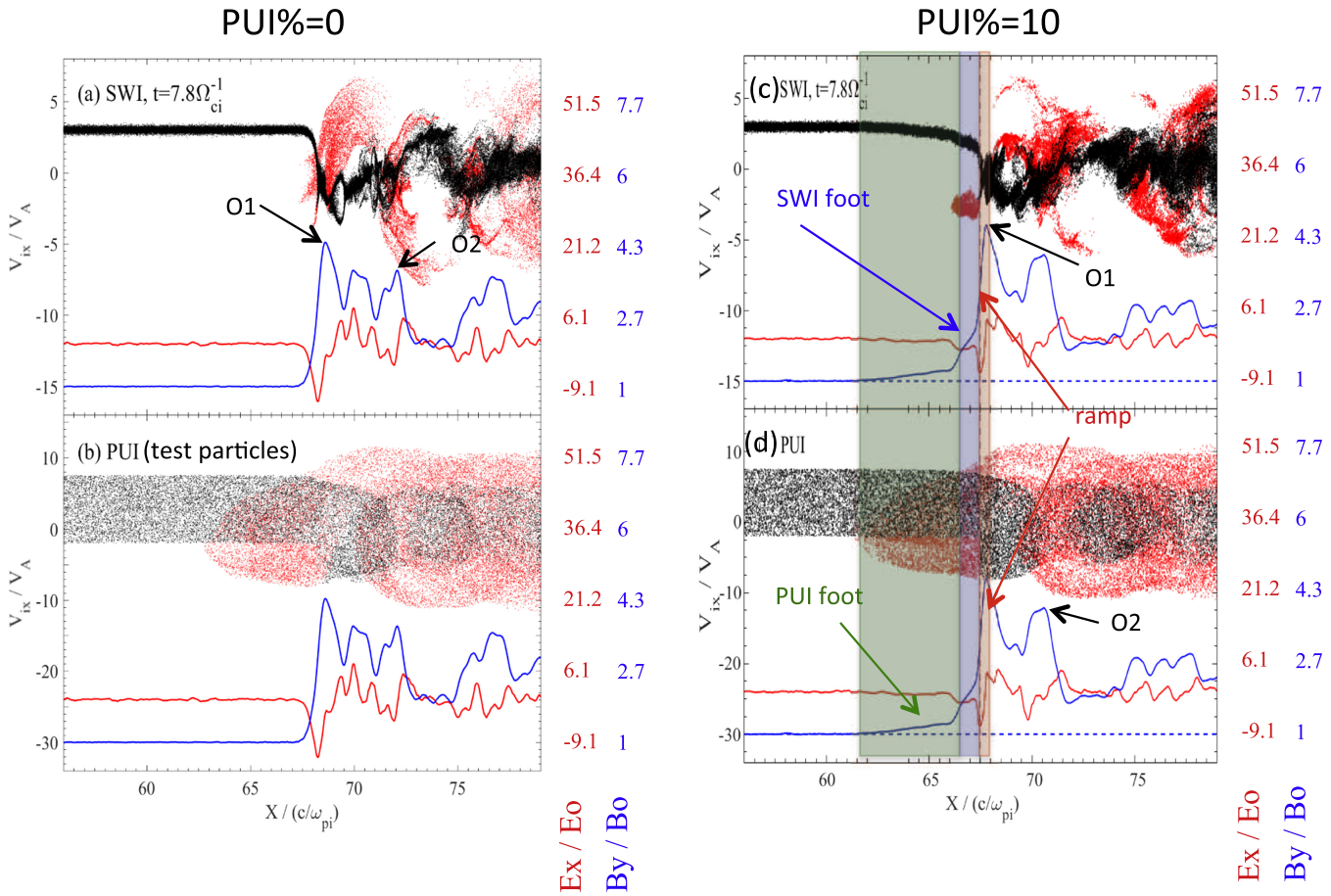

Figure 1. Phase space plots (x_i–v_{xi}) of the SWIs (top panels) and PUIs (bottom panels) at the shock in the absence (PUI% = 0 used for reference) and presence of pickup ions (PUI% = 10, as in run 2) at time $t = 7.8\ \Omega_{ci}{}^{-1}$; in plot 1b, PUIs are test particles. The upstream incident ions (black dots) are separated into two populations at the shock front: reflected (red dots) and directly transmitted (black dots). In each panel, the main magnetic field B_y (blue curve) and the cross-shock electric field E_x (red curve) are shifted and shown for reference; values of particle velocity v_{xi} and of (B_y and E_x) fields are indicated, respectively, on the left- and right-hand vertical scales. PUI foot and SWI foot are highlighted by green and blue areas, respectively. The vertical dashed line indicates the ramp location where the amplitude of the electric field is maximum (used a reference); the ramp width is highlighted by a red area. Overshoots "O1" and "O2" are marked by the dark arrows.

left-hand side of the simulation box is $V_{inj} = 3$ for all present cases. The shock propagates toward the left-hand side with a velocity of ~1.78, i.e., the Alfvén Mach number M_A is about 4.78. Remember that the front self-reformation (due to the accumulation of reflected ions over a foot distance from the ramp) is a well known process and has been evidenced in 1D and 2D PIC simulations for a few decades (Biskamp & Welter 1972; Lembège & Dawson 1987; Lembège & Savoini 1992; Lembège et al. 2009), and has been largely analyzed in the absence of PUIs. In contrast with PIC simulations, the shock front nonstationarity was not analyzed (and not included) in previous hybrid simulations (Wu et al. 2009, 2010). One main reason is that the spatial resolution used therein (space grid $\Delta = 0.5\ c/\omega_{pi}$) was not high enough to initiate the self-reformation; then the smallest ramp thickness was limited to the space grid. Indeed, as shown by Hellinger et al. (2002), the spatial resolution needs to be higher (at least $\Delta < 0.5\ c/\omega_{pi}$) or lower depending on the β_i value) in the hybrid simulations, in order to get a stronger ramp steepening and to initiate the self-reformation self-consistently. In our present case (as in previous PIC simulations), the ramp thickness is much lower and reaches a few electron inertia lengths c/ω_{pe}.

For run 2 (PUI% = 10) shown in Figure 3(b), the measured M_A and cyclic period τ_{ref} of self-reformation are about 4.99 and 1.54 $\Omega_{ci}{}^{-1}$ respectively. Figure 3(c) shows that even in the presence of 25% PUIs (run 3), the shock front is still undergoing self-reformation, where the measured M_A and τ_{ref} are about 5.26 and 1.4 $\Omega_{ci}{}^{-1}$, respectively. It is worth noting that the self-reformation period of the shock front in the presence of PUIs becomes shorter. Indeed, the spatial width of SWI's foot is much smaller than the PUI foot, and new reflected SWIs see a "local" B_y field (defined for reference at the $\langle\langle$knee$\rangle\rangle$ between the SWIs and PUIs feet indicated by the arrow in Figure 4) with an amplitude higher than the far upstream B_o field. This $\langle\langle$local$\rangle\rangle$ amplitude is almost unchanged within one self-reformation for a given run (Figure 3) but increases as the percentage of PUIs increases as reported in Figure 7(e). As a consequence, the gyration of R-SWIs will be smaller. Figure 7(e) shows that the associated self-reformation period is (almost) linearly anticorrelated with the local amplitude of the B_{ty} field measured at the $\langle\langle$knee$\rangle\rangle$ in the PUI foot.

Another striking point is that the time-averaged upstream Alfvén Mach number M_A slightly increases as PUI% increases (Table 1). This result has been observed in previous PIC simulations (Chapman et al. 2005; Lee et al. 2005; Matsukiyo et al. 2007; Oka et al. 2011) but not explained yet. In order to clarify this question, we employ the multi-component

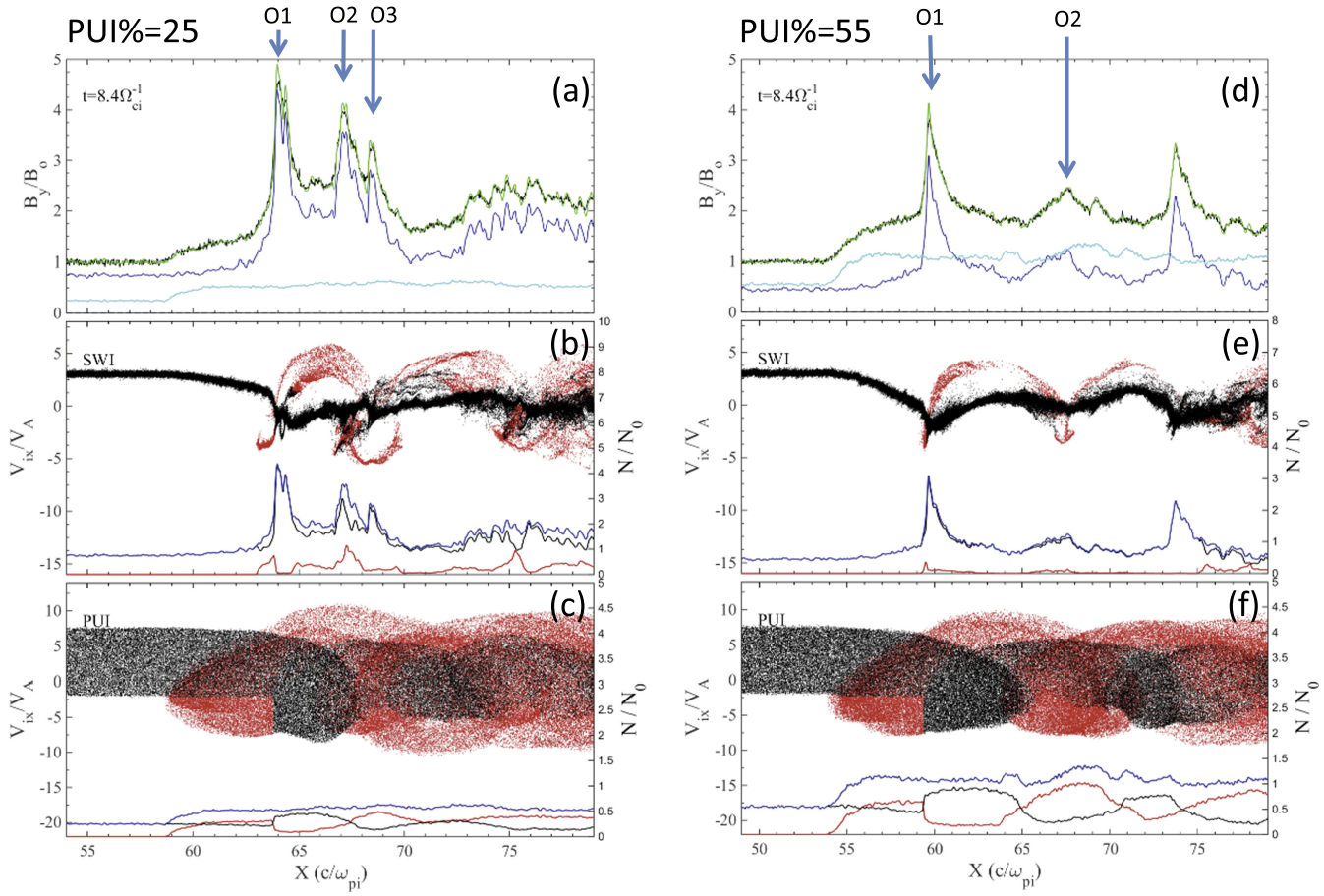

Figure 2. Profiles of the magnetic field B_y and the different ion density components at the shock front in the presence of 25% PUIs (run 3, left-hand column) and 55% PUIs (run 4, right-hand column). For each column, from top to bottom: (a) main magnetic field B_y/B_0 (dark curve), with density profiles of SWIs (blue curve), of PUIs (cyan), and total ion density (SWIs + PUIs, green curve); the left-hand *Y*-scale is the same for density and B_y profiles; (b) phase space plots of SWIs for R-SWIs (red dots) and DT-SWIs (black dots) with corresponding density profiles for R-SWIs (red curve), DT-SWIs (black curve), and total density of SWIs (R + DT, blue curve); *Y*-scale on the left- and right-hand side are, respectively, dedicated to the ion velocity component v_x and the density scale; (c) plot similar to (b) for PUIs. Arrows indicate the location of the overshoots "O1," "O2," and "O3."

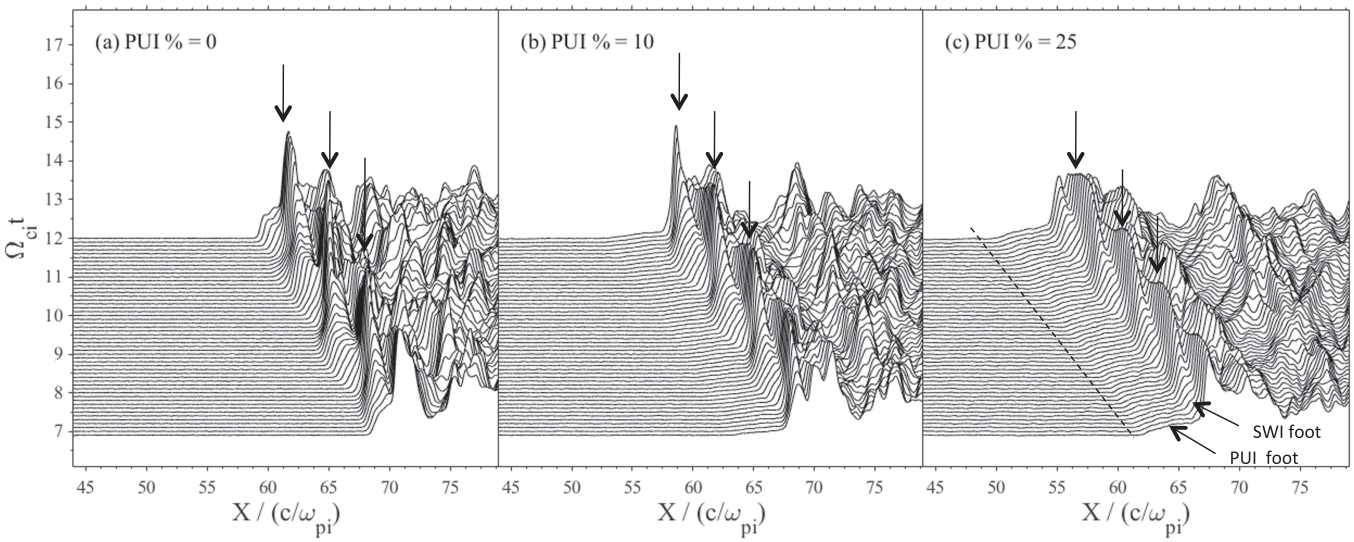

Figure 3. Time stackplots of the main magnetic field B_y, for three simulations at various relative densities of PUIs: (a) 0% (run 1), (b) 10% PUIs (run 2), and (c) 25% PUIs (run 3). All simulations correspond to a moderate Mach regime around $M_A \sim 5$ (precise values are given in Table 1). In each panel, successive large amplitude overshoots "O1" are marked by vertical arrows. The dashed line in panel (c) shows the leading edge of the PUI foot.

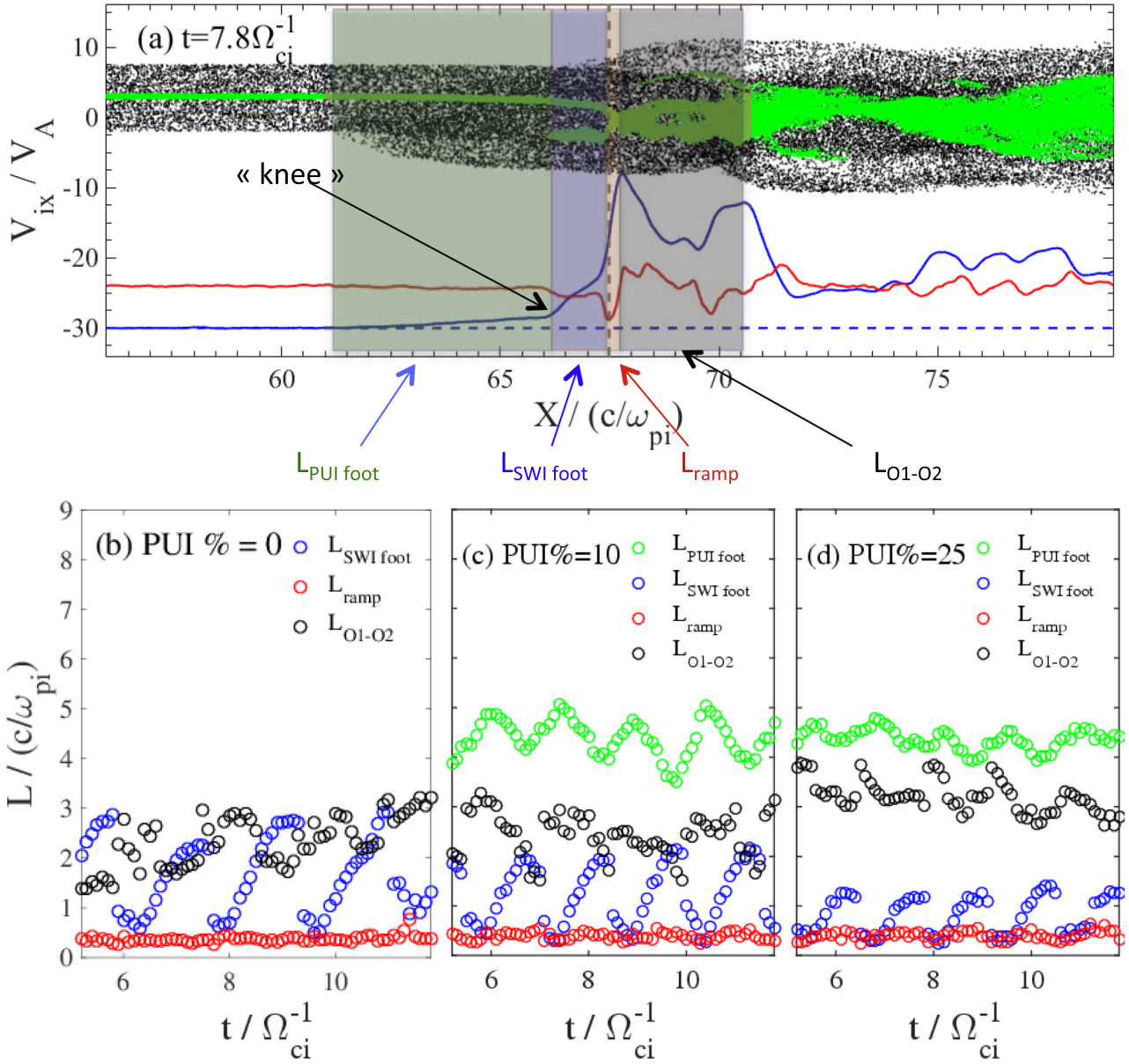

Figure 4. (a) Phase space plots of PUIs (black) and SWIs (green) for run 2 (PUI% = 10) at a fixed time $t = 7.8\ \Omega_{ci}^{-1}$. The main magnetic component B_y (blue curve) and cross-shock electric field E_x (red curve) are also shown for reference. The widths of PUI foot, SWI foot, ramp, and the distance between the two overshoots ("O1" and "O2") are highlighted in green, blue, red, and gray respectively. Time-evolution of these widths at the different shocks obtained with different percentages of PUIs: (b) 0% (run 1), (c) 10% (run 2), and (d) 25% (run 3). All simulations correspond to a moderate Mach regime around $M_A \sim 5$. Different colored circles indicate the measured widths of the microstructures highlighted with the same colored bars used in the top panel.

Rankine–Hugoniot (R–H) Model proposed by Wu et al. (2009), which is based on the 1D hybrid simulation and the classical single-fluid R–H jump conditions in a magnetohydrodynamic shock. In their model, the downstream Alfvén Mach number $M_{A,d}$ can be obtained analytically in the shock rest frame $M_{A,d} = r_s^{-1.5}\ M_A$, where M_A is the upstream Mach number, and r_s is the compression ratio, which can be calculated by n_d/n_u, where n_d and n_u are plasma densities in the downstream and upstream regions. With the same M_A, the $M_{A,d}$ in the shock rest frame increases with the increasing PUI% (after Wu et al. 2009). We can deduce that, in the downstream frame (i.e., the simulation frame widely used in previous PIC simulations of the TS), the shock front propagates faster relative to the downstream plasma for the higher PUI% case, as the V_{inj} is kept unchanged. This suggests that the upstream bulk energy transfer to SWIs is lower for the shock in the presence of PUIs since it goes mainly to PUIs, and there is less need for local dissipation of SWIs at the front. Thus, the shock can go faster and the downstream compression ratio of SWIs becomes lower (i.e., r_s becomes smaller). Our simulation results are consistent with the multi-component R–H Model.

Third, we study the impact of the self-reformation on the spatial scale lengths of shock front microstructures: PUI foot, SWI foot, ramp, and the separation distance between overshoots "O1" and "O2." Scale lengths of the front microstructures are identified in Figure 4(a). The PUI foot scale (highlighted in green) is measured from the upstream edge of the PUI foot (determined by the fastest reflected PUIs) to the

leading edge of the SWI foot and is identified by green dots; the SWI foot scale (highligthed in blue) is measured from the upstream edge of the SWI foot (determined by the fastest reflected SWIs) to the upstream edge of the ramp and is identified by blue dots. The ramp scale (highlighted in red) is measured from the end of the SWI foot to the overshoot "O1." The whole ramp can be well fit by a straight line. The spatial scale of the distance between overshoot "O1" and overshoot "O2" (highlighted in gray) is measured from the first peak of B_y to the second peak in the immediate downstream; the locations of the overshoots are identified by comparing the density profiles (separately for each population) and magnetic profile (not shown here). Figures 4(b)–(d) show the time history of the different scale lengths for the PUI foot, SWI foot, ramp, and overshoot pairs (marked in the same color as the areas highlighted in Figure 4(a)) normalized to the upstream ion inertial length, over several self-reformation cycles. Results show that (1) the SWI foot and ramp scales are of the order of several ion and a few electron inertial lengths respectively (values are in Table 2); (2) the width of all microstructures fluctuates with a time period identical to the self-reformation cycle; in contrast, the ramp width is not affected by the self-reformation and stays unchanged for the different PUI% runs; (3) the width of the SWI foot is periodically changing in association with the self-reformation, and both its time-averaged value and the amplitude of the time fluctuations decrease as the PUI% increases; in contrast, the width of the PUI foot (green area) varies inversely to SWI foot and its time-averaged value is almost independent on the PUI%. However, these fluctuations do not compensate each other exactly so that the width of the total foot (SWI foot +PUI foot) is not constant (not shown herein) and slightly fluctuates in time even for the case of PUI% = 25; (4) the time varying width of the SWI foot can reach some low values comparable to that of the ramp for PUI% = 25 (Figure 4(d)); and (5) the time-averaged distance between the overshoots "O1" and "O2" increases with PUI%. These features may be helpful to indirectly identify the impact of PUI% in the downstream region of the TS, from the observed magnetic field data (if the Mach number is known).

Fourth, the impact of the self-reformation on the field amplitude for different PUI% is analyzed in Figure 5. The time variation of the maximum value $B_{y,max}$ (blue) measured at overshoot "O1," of the ratio of $B_{y,max}$ to the downstream averaged value B_{DS} (green), and of the maximum value of the cross-shock electric field $E_{x,max}$ (red) measured over several self-reformation cycles are shown in Figure 5(a) for run 1 (PUI% = 0). Similar results for runs 2 and 3 are shown in Figures 5(b) (PUI% = 10) and (c) (PUI% = 25), respectively. Results are summarized as follows. (1) As PUI% increases, the time variation of $B_{y,max}$ and $E_{x,max}$ persists, but the fluctuations' amplitude becomes weaker. (2) The time-averaged values of $B_{y,max}$ and $E_{x,max}$ decrease as PUI% increases; then, since the cross-shock potential becomes lower, more directly transmitted SWIs and PUIs are expected for higher PUI% case, which has been confirmed in previous PIC simulations (Matsukiyo & Scholer 2011; Yang et al. 2012a). (3) Only the time-averaged value of the downstream ratio $B_{y,max}/B_{DS}$ (green) is almost independent of PUI%.

Finally, at the end of this section, we investigate the impact of the self-reformation on the instantaneous velocity of the shock front (measured at the ramp location). Figure 6 shows the

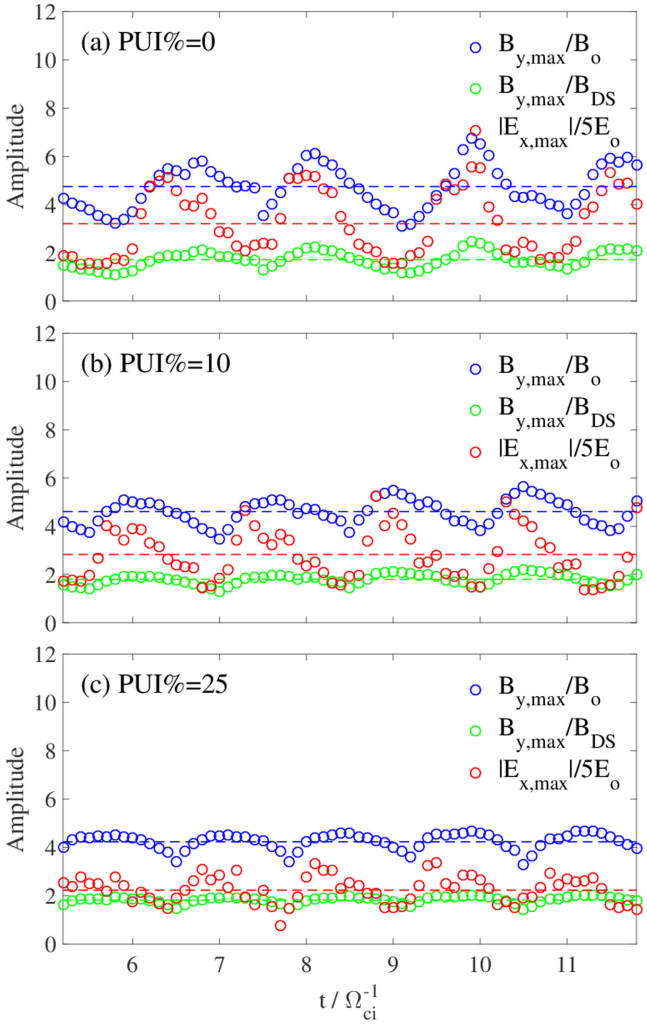

Figure 5. Time-evolution of the maximum values of $B_{y,max}/B_0$ (blue circles) at the shock front (overshoot "O1") where B_o (=B_{oy}) is the upstream magnetostatic field, of the ratio $B_{y,max}/B_{DS}$ (green circles, where B_{DS} is the downstream averaged value of the magnetic field amplitude), and of the maximum of cross-shock electric field $E_{x,max}/5E_0$ (red circles) at different shocks obtained with different PUI%: (a) 0% (run 1), (b) 10% (run 2), and (c) 25% (run 3); $E_o = V_{inj}\, B_o$ is the conduction field, where V_{inj} is the injection velocity along the x-axis. All simulations correspond to a moderate Mach regime around $M_A \sim 5$. In each panel, horizontal dashed lines indicate the time-averaged amplitude of these maximum values during the self-reformation.

time evolution of this velocity normalized to the upstream V_A (i.e., the instantaneous Alfvén Mach number V_{Shock}/V_A, left-hand side scale) and to the upstream ion thermal velocity V_{thi} for different PUI% runs (right-hand-side scale); in each panel, the black horizontal dashed line indicates the values of the instantaneous velocity averaged over several self-reformations (these values are used to define the Mach regime of each shock as reported in the runs of Table 1). Note that the foot is considered to be a "new" ramp (cross) when its local amplitude (growing during the self-reformation) becomes large enough to start reflecting new incoming ions. This takes place simultaneously as the "old" ramp (circle) still continues to reflect some ions that have succeeded to pass through the "new" ramp during the growth of the foot. This explains why within a small timescale (illustrated by a gray bar within one reformation cycle), two corresponding values of V_{Shock} are reported since these are defined for the "old" and the "new" ramp respectively

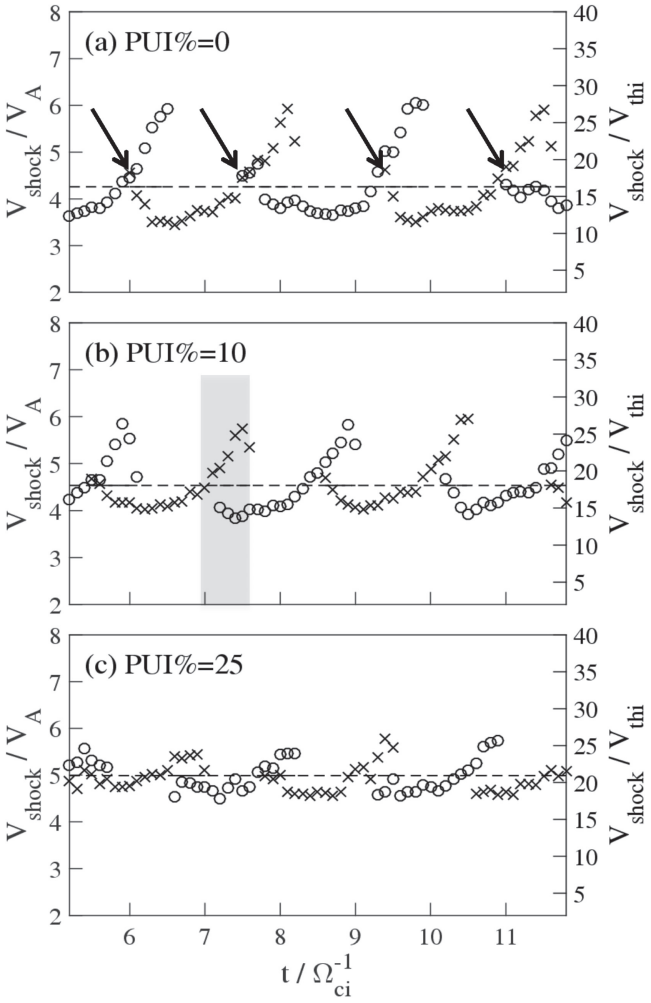

Figure 6. Time-evolution of the instantaneous shock front velocity measured at the ramp (vertical dashed line in Figure 1) for different shocks with different PUI%: (a) 0% (run 1), (b) 10% (run 2), and (c) 25% (run 3). All simulations correspond to a moderate Mach regime around $M_A \sim 5$. In each panel, the black horizontal dashed line indicates the shock velocity averaged in time (over successive self-reformations); this time-averaged value is used for providing the Mach regime of the shock for each run. Circles correspond to the time evolution of one ramp from the time it is identified as a foot starting to reflect new incoming ions (so called "new" ramp) until the time it vanishes out further downstream (so called "old" ramp); crosses correspond to the next ramp and so on alternatively. Arrows indicate the time when the measurement is made from the "new" ramp for the case PUI% = 0 used as reference (panel a). The gray bar (panel b) illustrates the time range where the instantaneous velocity can be identified from both "old" and "new" ramps.

(more exactly at the location of the maximum electric field E_{max} value, which is used as reference within the ramp). Later on (i.e., after this time range), the "old" ramp vanishes out further downstream and no associated V_{Shock} value can be defined; only the "new" ramp persists with its associated instantaneous velocity V_{Shock}. The co-existence of the "old" and "new" ramps explains the alternance of crosses and circles used within each panel between the successive self-reformation cycles. Figure 6 evidences the following points. (1) The instantaneous velocity strongly varies in time by almost a factor two for PUI% = 0%. (2) this variation decreases as the PUI% increases. (3) the value of the instantaneous velocity averaged over several self-reformation (dashed line) increases with PUI%, which is in good agreement with the multi-component R–H Model mentioned above. Recall that in all cases the ratio V_{Shock}/V_{thi} remains high (>15), which is in favor of the self-reformation as shown by Scholer et al. (2003); this criterium is equivalent to low β_i conditions as invoked by Hada et al. (2003).

4. SIMULATION RESULTS: IMPACT OF A HIGHER MACH NUMBER ($M_A \sim 9$)

In this section, we address the same questions as in Section 3, but now for shocks with a higher M_A regime. Results of runs 5–7 (with $M_A \sim 9$) are compared with the results of runs 1–3 ($M_A \sim 5$) shown in Section 3. The bottom panels in Figure 7 show the time stackplots of the main magnetic field B_y for shocks in runs 5 (PUI% = 0) and 7 (PUI% = 25), respectively. In the upper panels, results from the moderate Mach number case ($M_A \sim 5$) are shown for reference. Results show that (1) the self-reformation persists in the 25% PUIs case but the fluctuation amplitude is amplified for the high M_A regime (Figure 7(d)), and (2) in other words, high M_A regime compensates for the smoothing of field variations (to compare Figures 7(a) and (b)) due to the presence of PUIs. Moreover, previous works have evidenced that the features of self-reformation are controlled by several factors (Lembège & Dawson 1989; Lembège & Savoini 1992; Hada et al. 2003; Scholer & Matsukiyo 2004; Lembège et al. 2009; Matsukiyo & Scholer 2014), and no existing theory can be used to describe the combined impact of the shock propagation angle Θ, of the M_A regime, of the upstream β_i and of PUI% on the self-reformation process. In Figure 7(e), we examine the self-reformation period for moderate M_A (runs 1–4: circles) and high M_A (runs 5–8: crosses) cases as a function of PUI%. As the percentage PUI% increases, the self-reformation becomes faster in high M_A cases as well as in moderate M_A cases. For the moderate $M_A \sim 5$, field amplitudes at the front are too weak (field smoothing is too strong) to feed the reflection of a noticeable percentage of SWIs for the case PUI% = 55, and no self-reformation can take place.

Figure 8 shows a comparison of the impact of PUI% on the widths of the shock microstructures for moderate M_A (upper panels) and high M_A (bottom panels) cases. As M_A increases in the presence of 25% PUIs, (1) the amplitude of variations $\Delta L_{PUI\ foot}$ and $\Delta L_{SWI\ foot}$ becomes larger, and these variations become so large that values of $L_{SWI\ foot}$ approach $L_{PUI\ foot}$ foot during a reformation cycle and (2) the width variations of the SWI and PUI feet are still time anticorrelated with each other. The shock ramp width is an important criteria for the particle acceleration mechanisms, especially for efficiency of the shock surfing acceleration (Lee et al. 1996; Zank et al. 1996; Shapiro & Ucer 2003). Figures 8(e) and (f) show that, whatever the time and for PUI% = 0, the width of the shock ramp stays within the range of 2.5–4 c/ω_{pe} in the moderate M_A case, and is almost unchanged for high M_A. As both the PUI% and M_A increase, the ramp width is almost not affected by the presence of PUIs and still stays around a few c/ω_{pe}; for high M_A, the ramp width only varies within the range of $3c/\omega_{pe}$ to $7c/\omega_{pe}$ for the 25% PUI case.

The maxima amplitudes $B_{y,max}$ (blue) and $E_{x,max}$ (red) measured within the shock front are time-evolving during the self-reformation, and their time-averaged values decrease as the

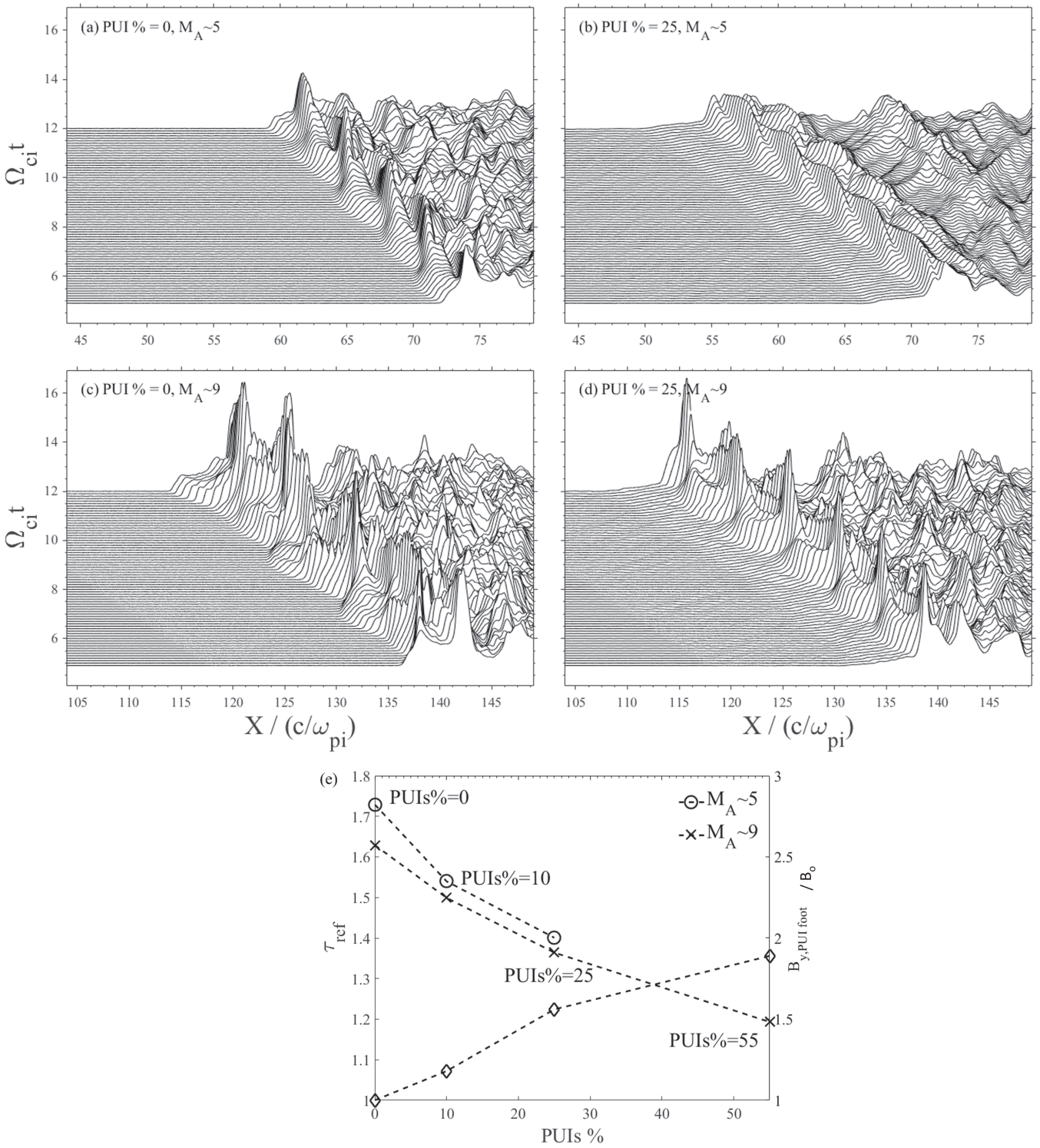

Figure 7. Time-stackplots of the main magnetic field B_y at different shocks. The upper panels correspond to shocks obtained for different percentages of PUIs: (a) 0% (run 1) and (b) 25% (run 3) for the moderate Mach number case ($M_A \sim 5$); bottom panels are for corresponding shocks ((c) run 5, and (d) run 7) obtained for the high Mach number case ($M_A \sim 9$). The variation of the front self-reformation period T_{ref} vs. the relative percentage of PUIs for moderate M_A (circles, runs 1–4) and high M_A (crosses, runs 5–8) regimes is shown in panel (e); no self-reformation is observed for run 4. For each case, the value of T_{ref} is averaged over 4–5 self-reformation cycles. The local amplitude of the $B_{y,PUI\ foot}$ field is measured at the $\langle\langle$knee$\rangle\rangle$ in the PUI foot (see the text and the arrow in Figure 4(a)) with the scale on the right-hand vertical axis and is reported (diamond) in Figure 7(e); for each run, this local amplitude has been time-averaged over one self-reformation cycle.

PUI% increases in both moderate and high M_A cases (Figure 9). As M_A increases, the amplitude of $B_{y,max}$ and $E_{x,max}$ fluctuations becomes larger. Figure 6 has shown that for the moderate M_A regime, the time variation of the instantaneous shock velocity becomes weaker in the presence of 25% PUIs. Additional results (similar to plots of Figure 6 but not shown herein) performed for high M_A case show that (1) the time-averaged velocity value $\langle V_{Shock}\rangle$ increases with M_A (Table 1) from $\langle V_{Shock}\rangle/V_A = 5.26$ (run 3) to 9.11 (run 7) and (2) the time variation of this velocity becomes much larger (V_{Shock}/

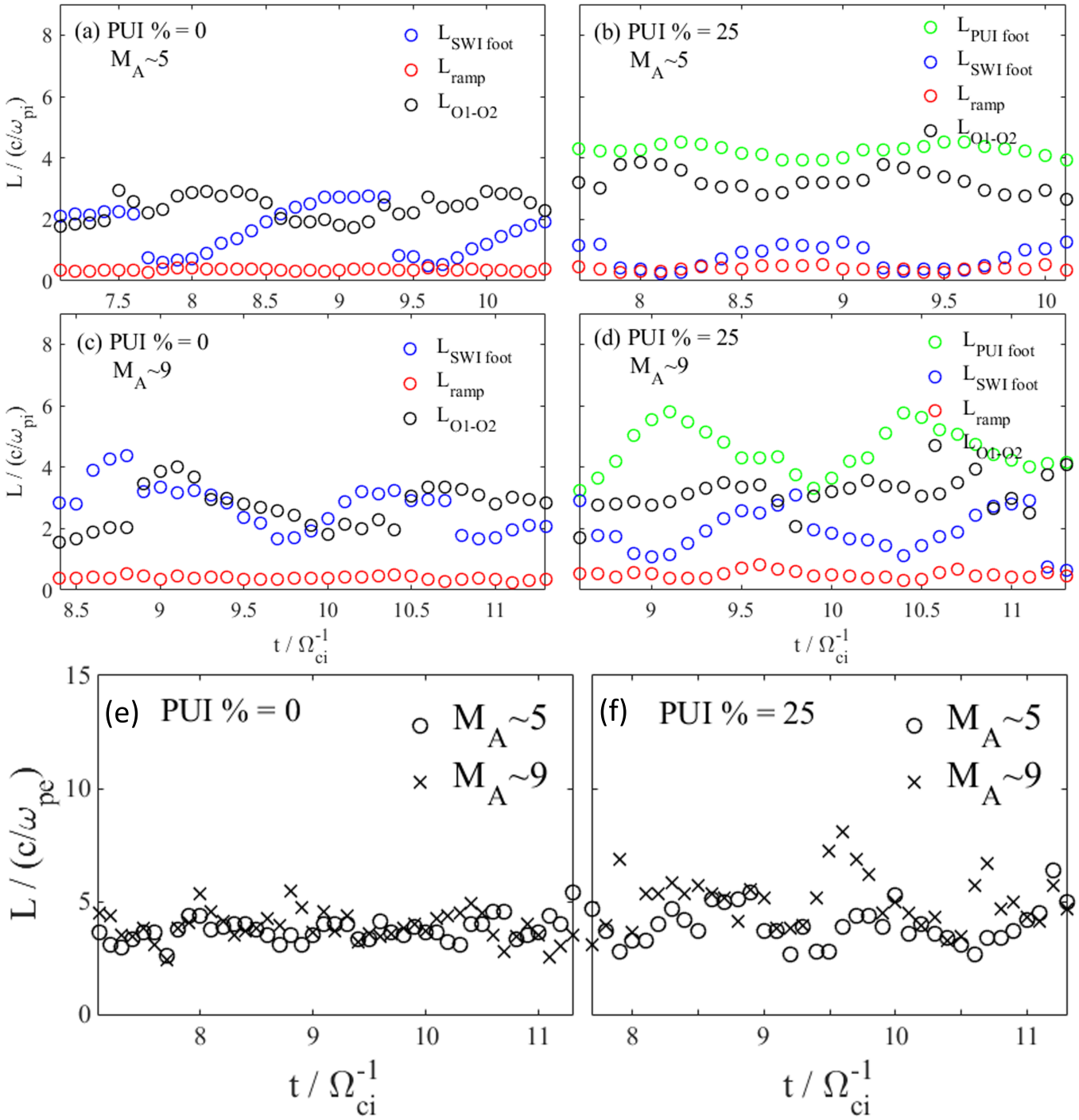

Figure 8. Time history of the widths of the PUI foot (green), SWI foot (blue), ramp (red), and the distance L_{O1-O2} (black) defined between overshoots "O1" and "O2" over several self-reformations. Top panels are for the moderate Mach number regime ($M_A \sim 5$) [(a) run 1, PUI% = 0 (used for reference), and (b) run 3, PUI% = 25], and bottom panels are for the high Mach number regime ($M_A \sim 9$) [(c) run 5, PUI% = 0, and (d) run 7, PUI% = 25]. The time history of the ramp thickness (normalized vs. the electron inertia length c/ω_{pe}) for shocks in the presence of 0% PUIs and 25% PUIs over several self-reformations is shown, respectively, in panels (e) and (f); in each panel, results are obtained for the moderate ($M_A \sim 5$, marked by circles) and high ($M_A \sim 9$, marked by crosses) Mach number regimes.

$V_A = 4.5$–5.8 for $M_A \sim 5$) (Figure 6(c)), and 6.8–10.8 for $M_A \sim 9$ respectively). This confirms that high M_A regime is in favor of shock front multi-crossings.

5. SWI-DOMINATED (25% PUIS) SHOCK VERSUS PUI-DOMINATED (55% PUIS) SHOCK.

Matsukiyo & Scholer (2011) found that in an extreme pickup ion-dominated case (PUI% = 60) the cross-shock potential reaches a maximum value in the extended PUI foot and decreases when approaching the magnetic field overshoot "O1." However, for a perpendicular shock and a fixed β_i, the persistence or the disappearance of the self-reformation depends on both combined parameters: the M_A regime and the percentage PUI% in particular in such extreme cases, which has not been mentioned before. In this section, we numerically investigate this dependence. Figure 10 compares the results

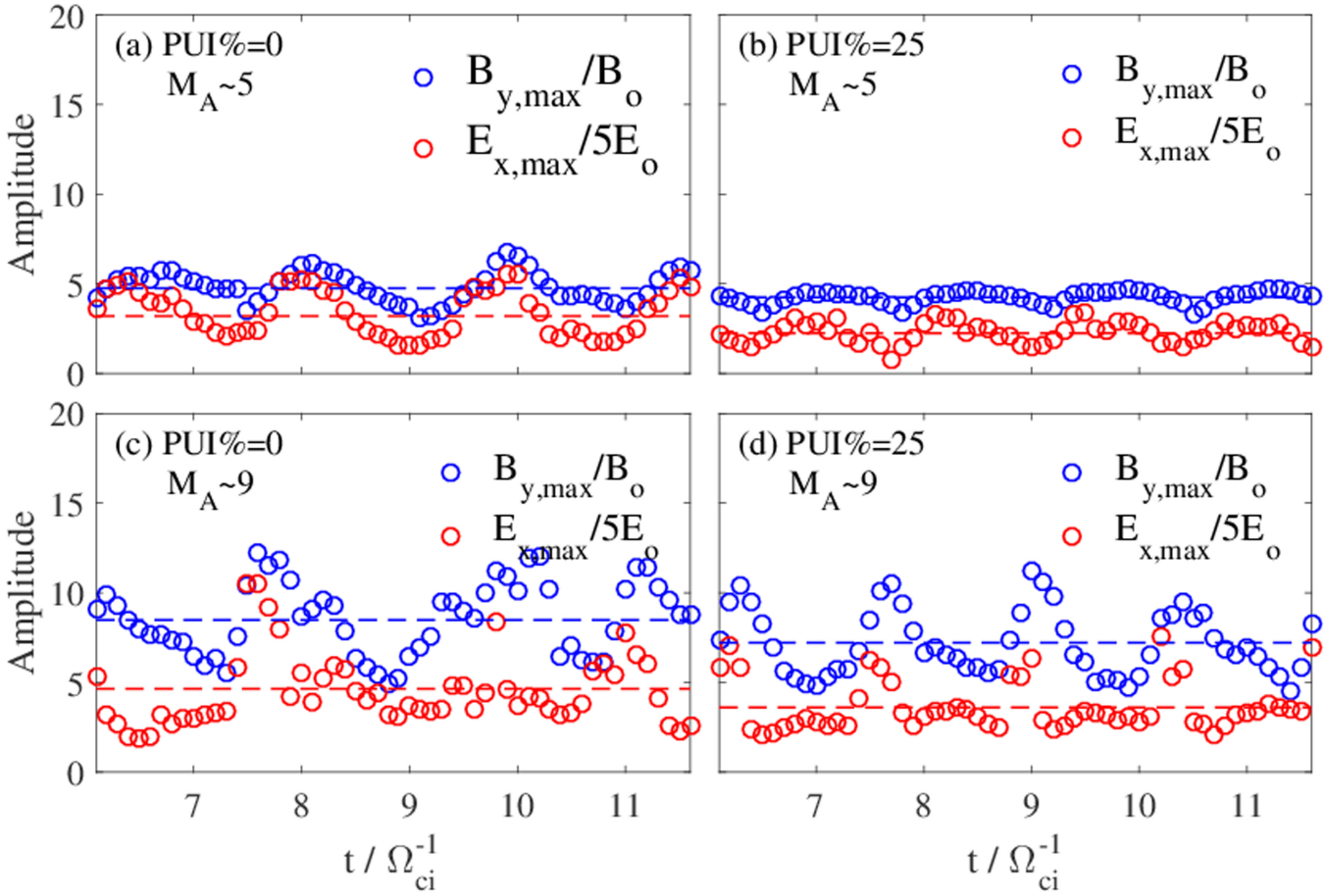

Figure 9. Time-evolving amplitudes of the magnetic peak $B_{y,max}$ (measured at the overshoot "O1") and the cross-shock electric field $E_{x,max}$ (measured within the ramp) over several self-reformations. Top: values of $B_{y,max}/B_0$ (blue) and $E_{x,max}/5E_0$ (red) of different runs [(a) run 1, PUI% = 0, and (b) run 3, PUI% = 25] in the moderate Mach number regime ($M_A \sim 5$). Bottom: corresponding results of different runs [(c) run 5, PUI% = 0, and (d) run 7, PUI% = 25] in the high Mach number regime ($M_A \sim 9$). In each panel, the time-averaged values are indicated by horizontal dashed lines.

obtained for moderate ($M_A \sim 5$) and for high Mach number ($M_A \sim 9$), for PUI% = 25 (runs 3 and 7) and PUI% = 55 (runs 4 and 8). In the moderate M_A case (upper panels), Figure 10(a) shows that the overshoots "O1" (full arrow) and "O2" (dashed arrow) are time fluctuating because of the self-reformation, in the SWI dominated shock (PUI% = 25), while the shock front becomes stationary (both for overshoots "O1" and "O2") since the self-reformation disappears in the PUI dominated shock (PUI% = 55, in Figure 10(b)). In contrast, Figure 10(d) shows that the self-reformation still persists in the PUI dominated case (PUI% = 55) for high $M_A \sim 9$. The amplitudes of both overshoots are fluctuating, which means that in a large enough high M_A regime, the self-reformation can survive even in a PUI-dominated shock. Combining with results on the instantaneous shock velocity (Section 4), it is reasonable to deduce that quite different magnetic field shock profiles may be seen in a large M_A regime, even in the presence of a high percentage of PUIs (multi-shock crossing).

Snapshot of ion phase space and of the different ion density components are shown for the stationary shock (run 4) in Figure 2 (right column). It is clearly evidenced that the reflection rate of SWIs (i.e., the ratio N_{R_SWIs}/N_{SWIs} of reflected SWIs density over the total density of incident SWIs) is much weaker than for run 3 and is not strong enough to feed the self-reformation, which disappears; the foot in the R-SWIs density profile almost disappears, as it almost merges with the ramp as in Hada et al. (2003). Several features need to pointed out: (1) as the PUI% increases, the PUI foot amplitude increases while the amplitude of the overshoots ("O1" at the front and "O2" further downstream) in the B_y field decreases (to compare black curves in Figures 2(a) and (d)) as was already observed in previous works for quasi-perpendicular shock (Matsukiyo & Scholer 2011); (2) the decrease of "O1" amplitude persists whatever the time is as PUI% increases (Figure 5) and its amplitude is still only supported by DT-SWIs even for high PUI% (Figures 2(d)–(f)); (3) moreover, the location of "O2" identified in Figure 10(b) has been reported in Figure 2 (right column) which clearly evidences that the distance L_{O1-O2} largely increases in run 4 as compared with run 3, and all overshoots are mainly supported by the DT-SWIs except for the overshoot "O2" where the contribution of PUIs (in particular R-PUIs) becomes comparable to that of SWIs (cyan and blue curves in Figure 2(d)); and (4) the amplitude of the spatial anticorrelation between the R-PUIs and DT-PUIs profiles increases with PUI% (Figure 2(f)), which explains that the R-PUIs partially contribute to "O2" during their downstream gyromotion (to compare Figures 2(d) and (f)).

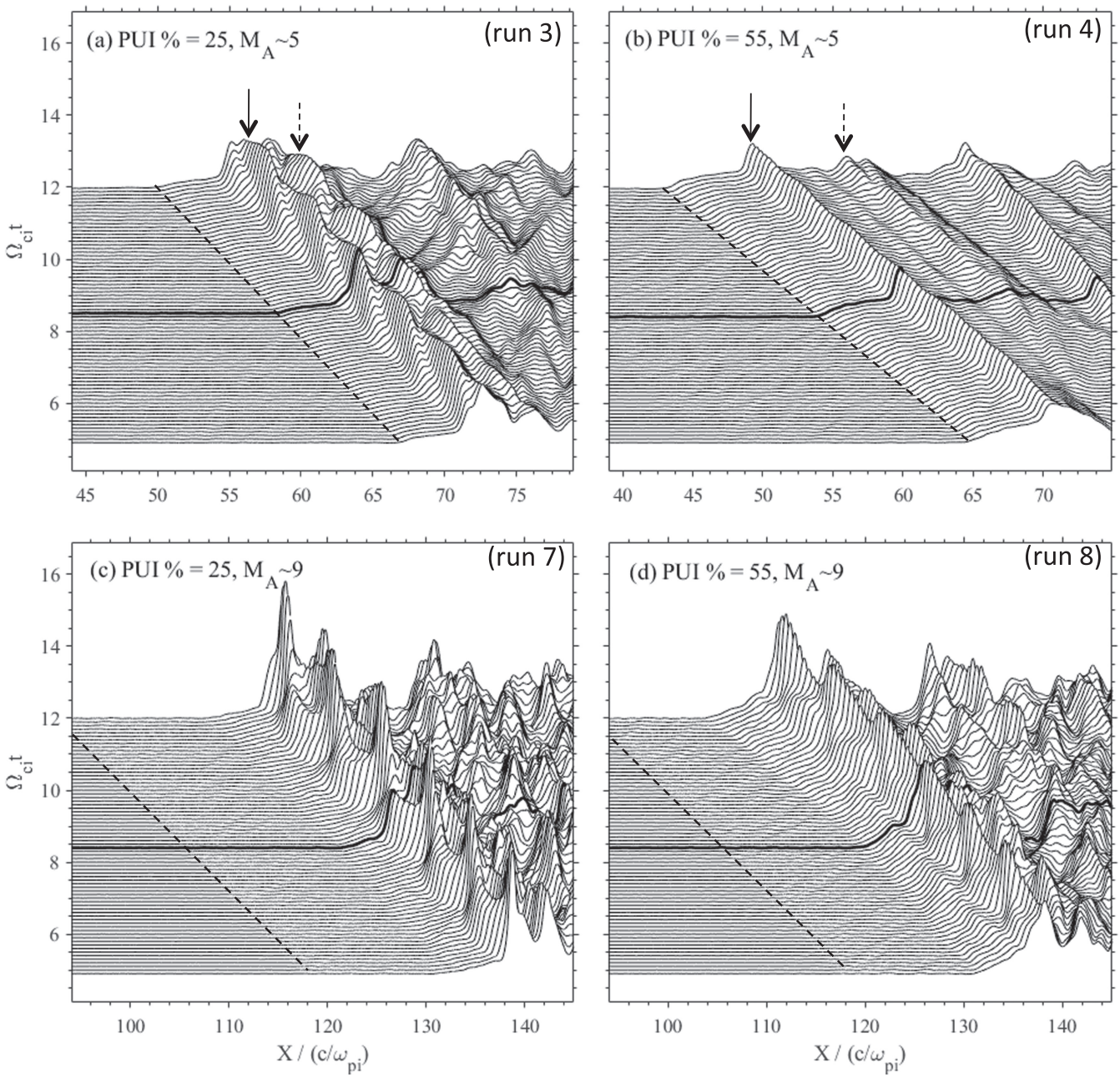

Figure 10. Time stackplots of the main magnetic field B_y at different shock conditions. Top: (a) run 3, PUI% = 25, and (b) run 4, PUI% = 55] in the moderate Mach number regime ($M_A \sim 5$). Bottom: corresponding results of different runs [(c) run 7, PUI% = 25, and (d) run 8, PUI% = 55] in the high Mach number regime ($M_A \sim 9$). In panel (a), the overshoots "O1" and "O2" are marked by full and dashed arrows, respectively. The dashed line indicates the upstream edge of the PUI foot. For comparison, the B_y profile is overlined with a thick full line at the time $t = 8.4\ \Omega_{ci}^{-1}$ which is also used as a reference time for Figure 2(a) (PUI% = 25) and Figure 2(d) (PUI% = 55).

6. IMPACT OF THE SHELL THICKNESS ON THE SHOCK FRONT NONSTATIONARITY

The modeled PUIs used in previous hybrid/PIC simulations are usually described by a thin-shell velocity distribution (zero thickness). Based on the early observations of PUIs in the solar wind, the distribution of PUIs is expected to be a partially-filled spherical shell since resulting from adiabatic cooling as the solar wind expands in the heliosphere (Vasyliunas & Siscoe 1976; Mobius et al. 1985, 1988; Burrows et al. 2010; Zank et al. 2010). Lee et al. (1996) mentioned that the thickness of the PUI velocity shell in different locations, such as at the cometary shock, the TS and on the corotating interaction region shock is quite different.

Herein, we analyze the impact of velocity shell thickness of PUIs on the microstructures and the nonstationarity of the TS in the presence of typical 25% PUIs. The upper panels in Figure 11 show the initial state of the PUI velocity shell distribution with different thicknesses $\delta = 0$, $0.2V_{shell}$, and $1V_{shell}$ as used in different runs (3, 9, and 11 respectively; to see Table 1). The middle panels show the corresponding time stackplots of the main magnetic field B_y for the moderate Mach number $M_A \sim 5$. Similar plots for the high Mach number

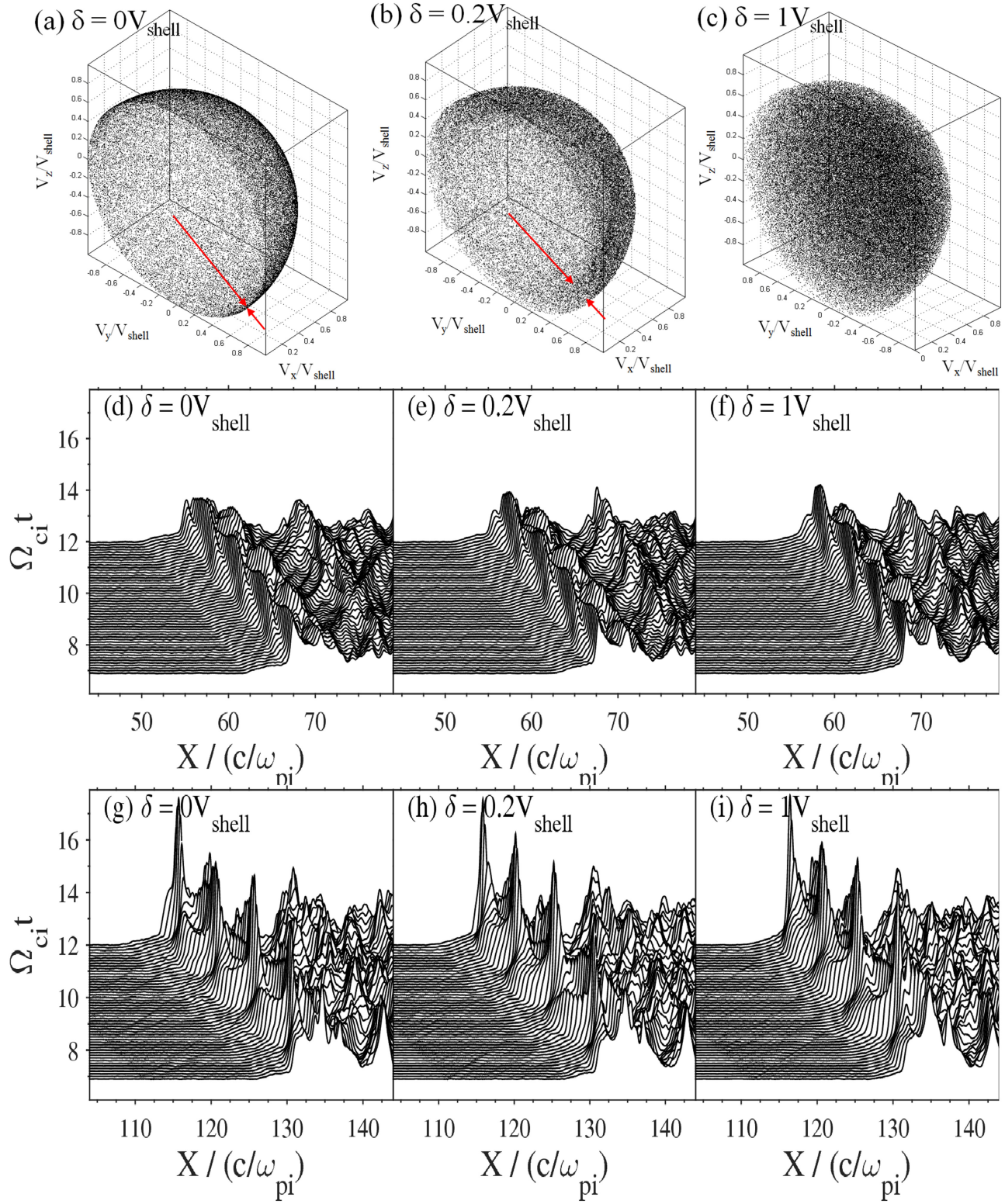

Figure 11. Top panels: 3D view of the cross-sections of the PUI velocity shell with different thicknesses: δ = (a) 0, (b) $0.2V_{\rm shell}$, and (c) $1V_{\rm shell}$. The shell thickness is marked by red arrows. Middle panels: corresponding time stackplots of $B_{\rm y}$ obtained for a fixed PUI% = 25 but with different shell thicknesses (runs 3 (d), 9 (e) and 11 (f)) in the moderate Mach number case ($M_{\rm A} \sim 5$). Bottom panels: similar plots as the middle panels (runs 7 (g), 12 (h) and 14 (i)) for the high Mach number case ($M_{\rm A} \sim 9$).

$M_{\rm A} \sim 9$ (runs 7, 12, and 14) are shown in the bottom panels; the cases $\delta = 0.5V_{\rm shell}$ are not shown herein (runs 10 and 13). Main results can be summarized as follows. (1) The impact of the thickness δ on the shock microstructures is not drastic for both moderate and high $M_{\rm A}$ cases (the maxima values of the fields overshoots and the microstructures scales remain almost unchanged). (2) The self-reformation persists for all cases. (3) However, results of Table 1 show that the $M_{\rm A}$ (i.e., of $v_{\rm Shock}$)

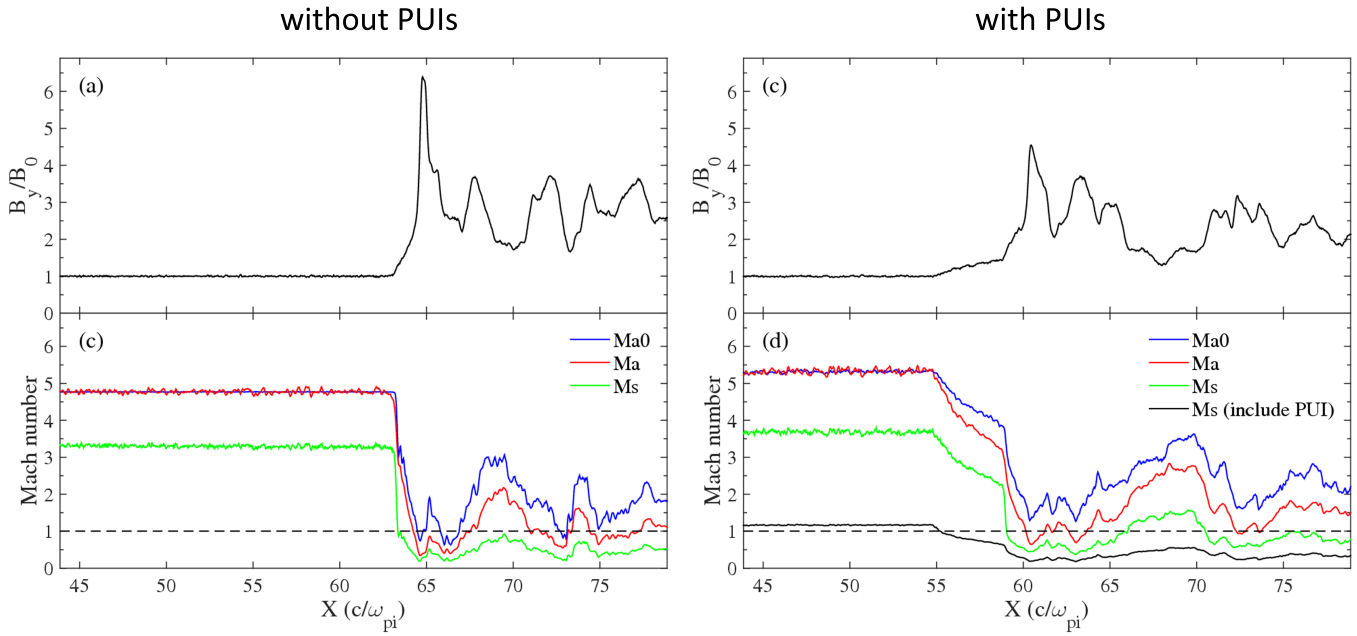

Figure 12. Profiles of the magnetic field B_y (upper panels) and Mach numbers (lower panels) for run 1 (left panels) and run 3 (right panels) at time $t = 10\,\Omega_{ci}^{-1}$. The blue and red curves show the Alfvénic Mach number obtained with the upstream Alfvénic speed and the local Alfvénic speed. Green and black curves show the magnetosonic Mach numbers obtained by using the magnetosonic speed defined without and with PUIs respectively.

value slightly decreases as δ increases. (4) The corresponding period T_{ref} of the self-reformation slightly increases with the shell thickness. (5) When approaching the front from upstream, the increase of the PUI foot (in both B_y and density profiles) is smoother as δ increases; this is due to the initial larger PUI diffusion in velocity space (similar to a warm population) for a finite δ, in contrast with the fact that PUIs are distributed within a very small part of the velocity space for $\delta = 0$ (at the edge of the shell), which is similar to a cold population. Then, even if the main features of the shock remain globally unchanged, the above features (3) and (5) may have some impact on the energy partition. This question is under active investigation and will be presented in a further paper. Then, results obtained in the previous simulations and present PIC simulation (based on zero thickness δ) can apply to the microstructures of the TS.

7. DISCUSSION

In order to clarify the present results with respect to previous works, the discussion of this section will focus on three points: (1) the downstream supersonic/subsonic regime, (2) the features of the shock front multicrossing, and (3) a comparison with previous works.

7.1. Downstream Supersonic/Subsonic Regime

Richardson et al. (2008) found that the fast-mode Mach number in the downstream region is still larger than one. This statement was a source of confusion, which is discussed here. Wu et al. (2009) mentioned that the plasmas instrument on *V2* does not accurately measure ions in the energetic tail of the velocity distribution (especially for the PUIs). Thus, the downstream Mach number is likely to be overestimated. Based on the multi-component R–H Model, they found that the downstream magnetosonic Mach number M_s in the shock rest frame is in a range from 0.55 (at $\gamma = 5/3$, where γ is the polytropic index) to 0.62 ($\gamma = 2.2$). Herein, we have examined the downstream Mach number by using self-consistent PIC simulations. The upper panels of Figure 12 show the magnetic main field B_y for run 1 (PUI% = 0) and run 3 (PUI% = 25) at time $t = 10\,\Omega_{ci}^{-1}$. The lower panels of Figure 12 show the flow Alfvén Mach number $M_{A0} = U/V_{A0}$ (U is the incident flow speed and $V_{A0} = 1$ is the upstream Alfvén speed), the local flow Alfvén Mach number $M_A = U/V_A$ (V_A is the local Alfvén speed), and the local magnetosonic Mach number $M_s = U/(V_A^2 + V_s^2)^{1/2}$ (V_s is the sonic speed which can be calculated excluding or including PUIs) in the shock rest frame. Figure 12(d) clearly evidences that the downstream plasma flow is super-Alfvénic (red curve) and well sub-magnetosonic (black curve) if the PUIs are included, in contrast with the case where PUIs are excluded (Figure 12(c)). We recover a transition from supersonic to subsonic regime at the TS shock as for any shock.

7.2. Interpretation of Multiple Crossings

When comparing with experimental data from *V2*, numerical results in Section 3 show that the variation of the instantaneous shock front velocity decreases for PUI% = 25. So, the front multicrossing becomes more difficult to be explained by the self-reformation alone. However, this result holds for a moderate Mach regime ($M_A \sim 5$). In contrast, for higher Mach number ($M_A \sim 9$), the time-variation of the instantaneous front velocity becomes larger, which is in favor of an easier multicrossing.

7.3. Comparison with Previous Works

7.3.1. Self-reformation Processes

Hada et al. (2003) have demonstrated that a high β_i value can suppress the self-reformation. Matsukiyo et al. (2007) have already investigated the impact of the mass ratio (m_i/m_e) used in the PIC simulation on the results, for an oblique (quasi-

perpendicular) shock. They concluded that the self-reformation is independent of the mass ratio and of the presence of (up to 10%) PUIs, although instabilities within the shock front (occurring in oblique shocks) strongly depend on these. We should keep in mind that the self-reformation in the present paper is due to the accumulation of R-SWIs over a foot distance from the ramp (as for perpendicular shock), while it can be due to the Modified Two Stream Instability (MTSI) excited by the relative drift between the R-SWIs/incoming SWIs and the incoming electrons, which requires a relatively high value of mass ratio and an oblicity of the shock propagation direction as in Matsukiyo et al. (2007). The present study is restricted to perpendicular shock propagation and the concerned self-reformation persists whatever the mass ratio is (Lembège et al. 2013); moreover, a combinaison of a high Mach number regime and/or a moderate PUI% is in favor of the self-reformation process and consequently of shock front multi-crossings.

7.3.2. Reflection Rate of SWIs and PUIs Populations

In a previous PIC simulation, Matsukiyo & Scholer (2011) qualitatively estimated that the fraction of PUIs at the shock front is almost 100%. Our results show that the reflection rate of SWIs (i.e., the ratio $N_{\mathrm{R\_SWIs}}/N_{\mathrm{SWIs}}$ of reflected SWIs density over the total density of incident SWIs) strongly decreases from 24.78%, to 16.81%, 8.95%, and 4.56%, as the PUI% increases from 0 to 10, 25 (TS conditions) and 55 (i.e., for runs 1 to 4 respectively). In contrast, the reflection rate of PUIs very slightly decreases 47.82% (test particles), to 47.77%, 47.44%, and 45.71%, as the PUI% increases from 0 (test particles) to 10, 25 (TS conditions) and 55 (i.e., for runs 1 to 4 respectively). In other words, the reflection rate of PUIs is almost independent of the PUI percentage. The decrease of both reflection rates is a consequence of the (time-averaged) field amplitude decrease at the shock front as PUIs% increases, and more SWIs and PUIs are expected to be directly transmitted. Note that the reflection rate mentioned herein is a time-averaged value, which is based on the separation method described in Section 1. We start counting the R ions and DT ions from a given time t_{A} ($=7\ \Omega_{\mathrm{ci}}^{-1}$) to a later time t_{B} large enough so that the time interval $\Delta t = (t_{\mathrm{B}} - t_{\mathrm{A}})$ contains several self-reformation cycles. The same time interval Δt is used for estimating the percentage of the different ion populations in the different runs; the time t_{B} corresponds to the end time of the simulation for all runs.

8. CONCLUSIONS

In this paper, we have used a 1D electromagnetic PIC code self-consistently including SWIs and PUIs in order to analyze the impact of PUIs on the microstructures and the self-reformation of the TS, and the retroaction of the self-reformation on PUIs and SWIs. A detailed analysis has been performed by separating each incident SWI and PUI population into two parts: reflected (R) and directly transmitted (DT). A parameter study has been performed to show the impact of different Mach number regimes and different velocity shell thicknesses of PUIs on the results. Present results can be useful for theoretical modelers of the TS microstructures, in order to analyze more precisely the energy partition and particle acceleration through the TS. Main results can be summarized as follows.

1. The self-reformation of the shock front persists quite well in the presence of a noticeable percentage of PUIs (25%) as that measured (indirectly) at the TS, and even for a moderate M_{A} regime.
2. The presence of PUIs has a strong impact on both the microstructures of the shock front and tends to smooth out the time fluctuations of field amplitude and of microstructure widths at the front and overshoots.
3. The TS has a multiple overshoot structure as confirmed by both *Voyager* observations and numerical simulations. B_{y} analyzing the contribution of the different ion densities (R and DT for each population), we found that the downstream microstructures of the shock front (overshoots) are mainly carrried by the gyrating DT-SWIs and very slightly by the R-SWIs further downstream for moderate PUI% (=25); no PUIs contribute. For high PUI% (=55), the dominant contribution of DT-SWIs still persists, except further downstream ("O2") where R-PUIs contribute to a certain amount.
4. For the moderate Mach regime, the amplitude of both overshoots "O1" and "O2" suffers noticeable periodic fluctuations due to the self-reformation even for PUI% = 25. When PUI% approaches 55, these time fluctuations disappear for both "O1" and "O2." However, for the high Mach regime, the overshoot fluctuations are recovered even for PUI% = 55. In other words, higher Mach regime compensates for the decrease of the field components at the front (and the resulting smoothing of the front self-reformation) as the percentage of PUIs increases.
5. As the PUI percentage increases, the shock becomes faster and the downstream compression ratio becomes weaker, which is explained by an R–H Model (Wu et al. 2009); in addition, the reflection rate of SWIs and PUIs decreases.
6. Present time stackplots of the main B field clearly evidence that the amplitude of the PUI extended foot increases with PUI%. The leading edge of the PUI foot roughly has a uniform motion with an almost constant velocity (equal to the time-averaged front velocity). The time variation of the PUI foot width confirms that it suffers the impact of the self-reformation, but its time-averaged value is almost unchanged for different PUI%. In contrast, as PUI% increases, the time-averaged width of SWI foot decreases slightly; the amplitude of its time fluctuations decreases but remains larger than those of the PUI foot width. In addition, the time variations of the PUI foot and SWI foot width are anticorrelated during a shock front self-reformation cycle; this feature is mainly due to the strong time variation of the upstream edge of the SWI foot rather than that of the PUI foot (uniform motion mentioned above).
7. PUIs are presently described by a zero thickness shell distribution. However, the shock structure does not seem to be sensitive to the choice of the shell thickness (a more precise assessment is underway and left for future work).
8. At the PUI dominated shock (PUI% = 55) and for moderate M_{A} (~5), the self-reformation disappears due to the limited percentage of R-SWIs (~4.56 %). The main process that allows the PUIs to stop the self-reformation process can be summarized as follows. The bulk velocity

of SWIs strongly decreases when these penetrate the PUI foot. As the SWIs reach the shock ramp, only a small fraction of incident SWIs is reflected due to their lower bulk velocity (as compared to the far upstream bulk velocity before these reach the PUI foot). Thus, the energy gain of the reflected SWIs at the shock front is reduced, and no clear vortex is formed in the SWI phase space (Lembège & Dawson 1987; Hada et al. 2003). So the self-reformation (fed by this vortex) is completely suppressed. However, for a higher M_A regime, the percentage of R-SWIs is large enough to feed the front nonstationarity, which persists even in the PUI = 55% case. In summary, the high Mach number regime allows us to compensate for the smoothing of the microstructures and the time fluctuations of the shock front brought by the presence of PUIs.

Present results focussed on the self-consistent shock front microstructures and the associated spatial/temporal scales variations can be helpful for modelers. In addition, the self-reformation analyzed presently provides a possibility for multi-crossings of the TS by *Voyager*. The higher dimensional effect on the self-reformation, the minority heavy ion effect on the shock microstructures, the self-excited front rippling effect on the precise shock front location (Lembège & Savoini 1992; Yang et al. 2012b), and the self-generated waves by the PUIs should be considered together in a further work. We also note that the upstream solar wind may include pre-existing large-scale turbulence (Lu et al. 2009; Guo & Giacalone 2010), so these waves may change the structure of the shock front and lead to a multiple crossings of the TS. The impact of the dynamic heliopause may also affect the location of the TS even if the upstream solar wind has a constant bulk velocity during the *Voyager* crossing. Such topics will be investigated in further works.

This research was supported by the National Science Foundation of China under grant No. 41574140, and in part by the Specialized Research Fund for State Key Laboratories of China. The computations were performed by Numerical Forecast Modeling R&D and VR System of State Key Laboratory of Space Weather and Special HPC work stand of Chinese Meridian Project.

REFERENCES

Axford, W. I. 1962, JGR, 67, 3791
Biskamp, D., & Welter, H. 1972, PhRvL, 28, 410
Burgess, D., Lucek, E. A., Scholer, M., et al. 2005, SSRv, 118, 205
Burgess, D., Wilkinson, W. P., & Schwartz, S. J. 1989, JGR, 94, 8783
Burlaga, L. F., Ness, N. F., Acuna, M. H., et al. 2008, Natur, 454, 75
Burrows, R. H., Zank, G. P., Webb, G. M., Burlaga, L. F., & Ness, N. F. 2010, ApJ, 715, 1109
Chapman, S. C., Lee, R. E., & Dendy, R. O. 2005, SSRv, 121, 5
Guo, F., & Giacalone, J. 2010, ApJ, 715, 406
Hada, T., Oonishi, M., Lembege, B., & Savoini, P. 2003, JGR, 108, 1233
Hellinger, P., Trávnícek, P., & Matsumoto, H. 2002, GeoRL, 29, 2234
Lee, M. A., Shapiro, V. D., & Sagdeev, R. Z. 1996, JGR, 101, 4777
Lee, R. E., Chapman, S. C., & Dendy, R. O. 2005, AnGeo, 23, 643
Lembege, B., & Dawson, J. M. 1987, PhFl, 30, 1767
Lembege, B., & Dawson, J. M. 1989, PhRvL, 62, 23
Lembege, B., Giacalone, J., Scholer, M., et al. 2004, SSRv, 110, 161
Lembège, B., & Savoini, P. 1992, PhFlB, 4, 3533
Lembege, B., Savoini, P., Hellinger, P., & Travnicek, P. M. 2009, JGR, 114, A03217
Lembege, B., Yang, Z., & Lu, Q. 2013, AGUSM, 1801714, SM31A-2112
Liewer, P. C., Goldstein, B. E., & Omidi, N. 1993, JGR, 98, 15211
Lu, Q. M., Hu, Q., & Zank, G. P. 2009, ApJ, 706, 687
Matsukiyo, S., & Scholer, M. 2011, JGR, 116, A08106
Matsukiyo, S., & Scholer, M. 2014, JGR, 119, 2388
Matsukiyo, S., Scholer, M., & Burgess, D. 2007, AnGeo, 25, 283
Möbius, E., Hovestadt, D., Klecker, B., et al. 1985, Natur, 318, 426
Möbius, E., Klecker, B., Hovestadt, D., & Scholer, M. 1988, Ap&SS, 144, 487
Ness, N. F., Scearce, C. S., & Seek, J. B. 1964, JGR, 69, 3531
Oka, M., Zank, G. P., Burrows, R. N., & Shinohara, I. 2011, in AIP Conf. Proc. 1366 (Melville, NY: AIP), 53
Richardson, J. D., Kasper, J. C., Wang, C., Belcher, J., & Lazarus, A. J. 2008, Natur, 454, 63
Scholer, M., & Matsukiyo, S. 2004, AnGeo, 22, 2345
Scholer, M., Shinohara, I., & Matsukiyo, S. 2003, JGR, 108, 1014
Shapiro, V. D., & Ucer, D. 2003, P&SS, 51, 665
Stone, E. C., Cummlings, A. C., McDonald, F. B., et al. 2005, Sci, 309, 2017
Tidman, D. A., & Krall, N. A. 1971, Shock Waves in Collisionless Plasmas (New York: Wiley/Interscience)
Vasyliunas, V. M., & Siscoe, G. L. 1976, JGR, 81, 1247
Wu, P., Liu, K., Winske, D., et al. 2010, JGR, 115, A11105
Wu, P., Winske, D., Gary, S. P., Schwadron, N. A., & Lee, M. A. 2009, JGR, 114, A08103
Yang, Z. W., Han, D. S., Yang, H. G., et al. 2012a, Ap&SS, 341, 241
Yang, Z. W., Lembège, B., & Lu, Q. M. 2012b, JGR, 117, A07222
Yang, Z. W., Lu, Q. M., Lembège, B., & Wang, S. 2009, JGR, 114, A03111
Zank, G. P., Heerikhuisen, J., Pogorelov, N. V., Burrows, R., & McComas, D. 2010, ApJ, 708, 1092
Zank, G. P., Pauls, H. L., Carins, I. H., & Webb, G. M. 1996, JGR, 101, 457